Cell Reports

ASL Metabolically Regulates Tyrosine Hydroxylase in the Nucleus Locus Coeruleus

Graphical Abstract

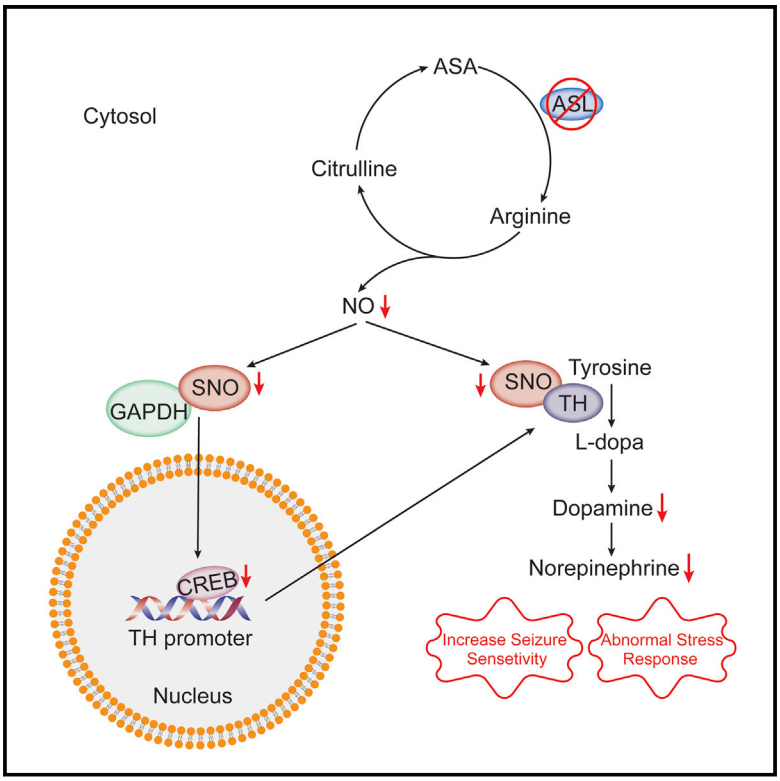

Authors

Shaul Lerner, Elmira Anderzhanova, Sima Verbitsky, ..., Sandesh C.S. Nagamani, Alon Chen, Ayelet Erez

Correspondence

ayelet.erez@weizmann.ac.il

In Brief

Lerner et al. show that ASL is expressed greatly in the nucleus locus coeruleus (LC), where it regulates NO levels. ASL deficiency in the LC of mice results in abnormal response to stress and in increased seizure sensitivity due to decreased TH activity and catecholamine synthesis. NO donors rescue the phenotype in LC-ASL-deficient mice.

Highlights

- ASL is expressed in the locus coeruleus (LC) and regulates catecholamine synthesis
- LC-ASL deficiency in mice promotes abnormal stress response and seizure sensitivity
- LC-ASL deficiency decreases nitric-oxide levels and tyrosine hydroxylase activity
- NO donors normalize catecholamine production and rescue LC-ASL deficiency phenotype

Lerner et al., 2019, Cell Reports *29*, 2144–2153
November 19, 2019
https://doi.org/10.1016/j.celrep.2019.10.043

CellPress

OPEN ACCESS
CellPress

Cell Reports
Report

ASL Metabolically Regulates Tyrosine Hydroxylase in the Nucleus Locus Coeruleus

Shaul Lerner,[1] Elmira Anderzhanova,[2,3] Sima Verbitsky,[4,5] Raya Eilam,[6] Yael Kuperman,[6] Michael Tsoory,[6] Yuri Kuznetsov,[6] Alexander Brandis,[7] Tevie Mehlman,[7] Ram Mazkereth,[8] UCDC Neuropsychologists, Robert McCarter,[9] Menahem Segal,[4] Sandesh C.S. Nagamani,[10,11] Alon Chen,[2,4] and Ayelet Erez[1,12,*]

[1]Department of Biological Regulation, Weizmann Institute of Science, Rehovot, Israel
[2]Department of Stress Neurobiology and Neurogenetics, Max Planck Institute of Psychiatry, Munich, Germany
[3]Clinic for Psychiatry and Psychotherapy, University Hospital Bonn, Bonn, Germany
[4]Department of Neurobiology, Weizmann Institute of Science, Rehovot, Israel
[5]Department of Biomedicine, University of Basel, Basel, Switzerland
[6]Department of Veterinary Resources, Weizmann Institute of Science, Rehovot, Israel
[7]Life Science Core Facility, Weizmann Institute of Science, Rehovot, Israel
[8]The Sackler School of Medicine, Tel-Aviv University, Tel-Aviv, Israel
[9]Center for Translational Sciences, Children's National Health System, The George Washington University, Washington, DC, USA
[10]Department of Molecular and Human Genetics, Baylor College of Medicine, Houston, TX, USA
[11]Texas Children's Hospital, Houston, TX, USA
[12]Lead Contact
*Correspondence: ayelet.erez@weizmann.ac.il
https://doi.org/10.1016/j.celrep.2019.10.043

SUMMARY

Patients with germline mutations in the urea-cycle enzyme argininosuccinate lyase (ASL) are at risk for developing neurobehavioral and cognitive deficits. We find that ASL is prominently expressed in the nucleus locus coeruleus (LC), the central source of norepinephrine. Using natural history data, we show that individuals with ASL deficiency are at risk for developing attention deficits. By generating LC-ASL-conditional knockout (cKO) mice, we further demonstrate altered response to stressful stimuli with increased seizure reactivity in LC-ASL-cKO mice. Depletion of ASL in LC neurons leads to reduced amount and activity of tyrosine hydroxylase (TH) and to decreased catecholamines synthesis, due to decreased nitric oxide (NO) signaling. NO donors normalize catecholamine levels in the LC, seizure sensitivity, and the stress response in LC-ASL-cKO mice. Our data emphasize ASL importance for the metabolic regulation of LC function with translational relevance for ASL deficiency (ASLD) patients as well as for LC-related pathologies.

INTRODUCTION

Argininosuccinate lyase (ASL) is a urea cycle enzyme that facilitates the conversion of excess nitrogen to urea in the liver. In extrahepatic tissues, ASL participates in the citrulline-arginine cycle to support the cellular requirement for arginine (Mori and Gotoh, 2004). In fact, ASL is the only enzyme in mammals that generates arginine although five other enzymes use arginine as a substrate for the synthesis of nitric oxide (NO), polyamines, agmatine, creatine, proline, and glutamate, all of which are essential for cell survival, growth, and proliferation (Mori and Gotoh, 2004). Loss of ASL would thus be predicted to affect multiple physiological processes. This is best illustrated by the complex phenotype observed in individuals with argininosuccinic aciduria or ASL deficiency (ASLD), a urea cycle disorder that is caused by germline, loss-of-function, pathogenic variants in *ASL* (Baruteau et al., 2017; Erez et al., 2011a; Mercimek-Mahmutoglu et al., 2010; Nagamani et al., 2011, 2012b; Tuchman et al., 2008). In spite of having fewer episodes of hyperammonemia as compared to individuals with other urea cycle disorders (UCDs), individuals with ASLD are at increased risk to develop intellectual and learning disabilities, behavioral abnormalities, epilepsy, ataxia, and hypertension (Baruteau et al., 2018; Brunetti-Pierri et al., 2009; Ficicioglu et al., 2009; Kho et al., 2018; Kleijer et al., 2002; Lågas and Ruokonen, 1991; Tuchman et al., 2000). Thus, pathogenic mechanisms other than hyperammonemia likely contribute to the phenotypes observed in ASLD.

We have previously reported that ASL is an essential regulator of systemic and tissue-specific NO production. Because of the structural necessity of ASL for the formation of a NO-synthesis complex, supplementation with arginine is not sufficient to replenish NO levels (Erez et al., 2011b). Treatment with pharmacologic precursors of NO rather than arginine have been shown to increase survival and correct hypertension in a murine model of ASLD. Interestingly, a patient with ASLD treated with NO supplements for hypertension also demonstrated beneficial effects on verbal memory and nonverbal problem solving (Nagamani et al., 2012a). Nitric oxide is a signaling molecule, which acts as messenger for multiple pathways in different tissues. In the CNS, NO has a role in various physiologic processes, including brain development, regulation of synaptic plasticity, and behavioral and physiology homeostasis (Bredt et al., 1990; Calabrese et al., 2007; Guix et al., 2005). Specifically, in the locus coeruleus (LC), NO is involved in synaptic transmission and the modulation of neuronal spiking and energy stability (Sanchez-Padilla et al., 2014; Xu et al., 1994). In the context of these

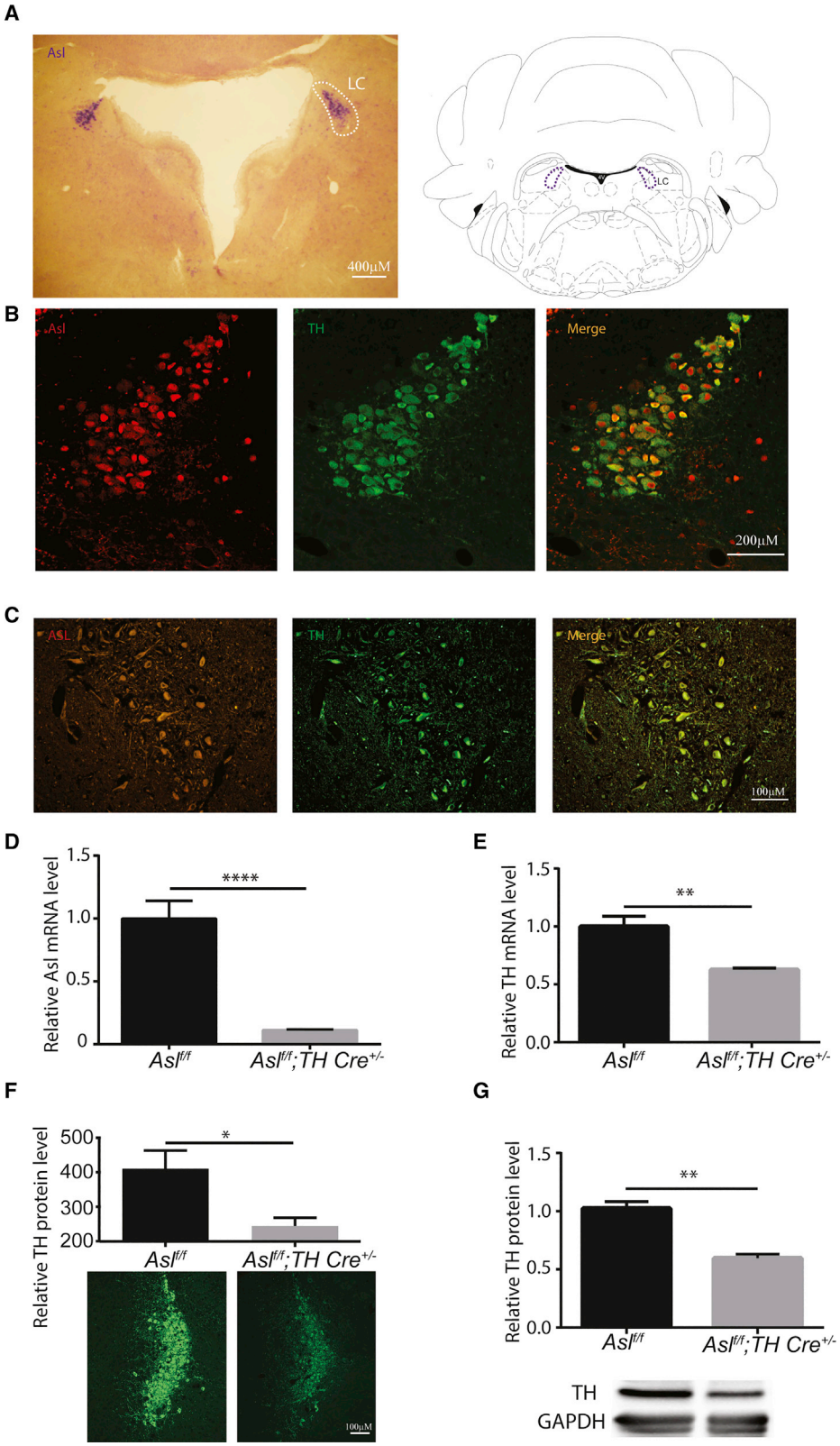

(legend on next page)

data, our aim was to understand the role of ASL and NO in the neurological phenotype in ASLD, as well as in neurobehavioral and cognitive functions.

RESULTS

ASL Is Highly Expressed in the Locus Coeruleus and Regulates TH Levels

To understand the roles of ASL in the brain, we first determined the distribution of ASL using *in situ* hybridization (ISH) and immunostaining in coronal sections of brain obtained from wild-type mice. Consistent with previous reports, we found sparse expression of ASL in different brain regions (Baruteau et al., 2018; Braissant, 2004); however, we found a prominent expression in the LC nuclei (Figures 1A and S1). In brainstem sections from mice as well as in brain tissue array from humans, we find ASL expression to distinctly co-localize with tyrosine hydroxylase (TH) expression, the gold standard for marking the LC region (Figures 1B and 1C). Interestingly, ASL expression in specific dopaminergic regions was faint (data not shown). To understand the role of ASL in the LC, we generated an ASL-LC conditional knockout (cKO) mouse by breeding $Asl^{f/f}$ mice with mice overexpressing Cre recombinase under the *TH* promoter ($Asl^{f/f}$;*TH* $Cre^{+/-}$) (Figure 1D). Using laser microdissections, we performed RNA sequencing, specifically on LC neurons collected from $Asl^{f/f}$ control and $Asl^{f/f}$;*TH* $Cre^{+/-}$ mice (Figure S2A; Table S1). Our analysis revealed prominent differences in pathways related to the stimulation and release of neurotransmitters from neurons, especially from the catecholamine nuclei (Figure S2B; Table S2). Interestingly, *TH* was among the most significantly differently expressed genes between the LC of $Asl^{f/f}$ control and $Asl^{f/f}$;*TH* $Cre^{+/-}$ mice, both at the mRNA and protein levels (Figures 1E–1G; Table S3). Notably, the decrease in TH was specific to $Asl^{f/f}$;*TH* $Cre^{+/-}$ mice and was not present in transgenic *TH* $Cre^{+/-}$ control mice (Figure S2C).

ASL Deficiency in Catecholamine Neurons Decreases Protein Nitrosylation

Because ASL has been shown to regulate NO synthesis (Erez et al., 2011b), we hypothesized that the reduction in TH levels in $Asl^{f/f}$;*TH* $Cre^{+/-}$ mice is caused by NO deficiency. We hence generated mice in which the LC neurons were labeled by the red florescence protein (RFP) dTomato ($Asl^{f/f}$,$Ai9^{f/f}$;*TH* $Cre^{+/-}$). Using flow cytometry, we found significantly lower NO levels in noradrenergic neurons of $Asl^{f/f}$,$Ai9^{f/f}$;*TH* $Cre^{+/-}$ mice in comparison to $Ai9^{f/f}$;*TH* $Cre^{+/-}$ control mice, although the RFP level did not differ between the groups (Figures 2A and S3A).

To evaluate the functional consequences of ASL and NO depletion on catecholamine neurons, we used the human neuroblastoma SH-SY5Y cells, which express both ASL and the proteins required for catecholamine synthesis. Following differentiation of SH-SY5Y cells to noradrenergic-like neurons with secretory activity (Kovalevich and Langford, 2013), we downregulated ASL expression using *shRNA* targeting *ASL* (Figures S3B and S3C). Corroborating the *in vivo* results, we found a significant downregulation of *TH* levels in differentiated SH-SY5Y neurons with *ASL* downregulation, as compared to *shGFP* control cells (Figure 2B). NO regulates its downstream effects, in part by protein nitrosylation, a post-translational covalent modification known to regulate protein activity (Foster et al., 2009). Specifically, nitrosylation of glyceraldehyde 3-phosphate dehydrogenase (GAPDH) affects the DNA binding ability of cyclic AMP (cAMP) response element-binding protein (CREB). CREB is one of the main transcription factors that regulate TH expression and its downstream effects (Harraz and Snyder, 2015; Tekin et al., 2014; Xu et al., 2013). GAPDH nitrosylation and expression of other CREB target genes (e.g., *cFOS* and *VGF*) were reduced in SH-SY5Y *shASL* neurons as compared to *shGFP* controls (Figures 2C, S3D, and S3E). In addition, direct nitrosylation of TH, which has been established to enhance its enzymatic activity (Wang et al., 2017), was also significantly reduced in *shASL* neurons (Figures 2C and S3D). Supplementing SH-SY5Y *shASL* neurons with NOS-independent NO donor normalized nitrosylation of both GAPDH and TH and increased *TH* mRNA levels similar to that of *shGFP* control neurons (Figures 2D, 2E, and S3F). Together, these results suggest that, following loss of ASL, the reduction in NO levels leads to reduced TH transcription and activity.

Decreased TH Is Associated with Impaired Catecholamine Synthesis

To test whether the downregulation of TH is functionally significant, we next examined catecholamine levels in LC of $Asl^{f/f}$;*TH* $Cre^{+/-}$ and $Asl^{f/f}$ control mice. Analysis of the neurochemical data showed that $Asl^{f/f}$;*TH* $Cre^{+/-}$ had decreased norepinephrine and dopamine levels (Figure 3A). Because clinical manifestations as attention deficits and anxiety related to LC pathogenicity have been shown to involve an abnormal catecholamine release in response to stress (McCall et al., 2015), we measured catecholamine levels following stressful stimuli. Following acute stress provocation, dopamine levels

Figure 1. ASL Is Highly Expressed in the LC and Regulates TH Levels

(A) Left: *in situ* hybridization with *Asl* anti-sense mRNA probe showing in purple *Asl* prominent expression in the LC. Right: scheme of brain stem coronal section is shown. LC region is highlighted in purple (image adapted from The Mouse Brain Atlas).

(B) Immunostaining of mouse brainstem for Asl (left, red), TH (center, green), and their merged co-localization (right).

(C) Immunostaining of human brainstem for ASL (left, red), TH (center, green), and their merged co-localization (right).

(D and E) Quantification of *Asl* mRNA (D) and *TH* mRNA (E) isolated by laser microdissection from the LC of $Asl^{f/f}$;*TH* $Cre^{+/-}$ and from $Asl^{f/f}$ control mice as measured by RT-PCR with specific TaqMan probes (n = 100 cells from 7 animals).

(F) Immunohistochemistry quantification of TH protein normalized to cells number (n = 4 in each group).

(G) Quantification of western blots for TH levels in LC regions taken by punch biopsies (n = 4 in each group).

The bottom panels of (F) and (G) show representative images for each detection method, respectively.

Data represent mean ± SEM (*p < 0.05; **p < 0.01; ***p < 0.001; ****p < 0.0001; ns, not significant). See Tables S1, S2, and S3 for RNA sequencing, ingenuity pathway analysis, and proteomic analysis, respectively.

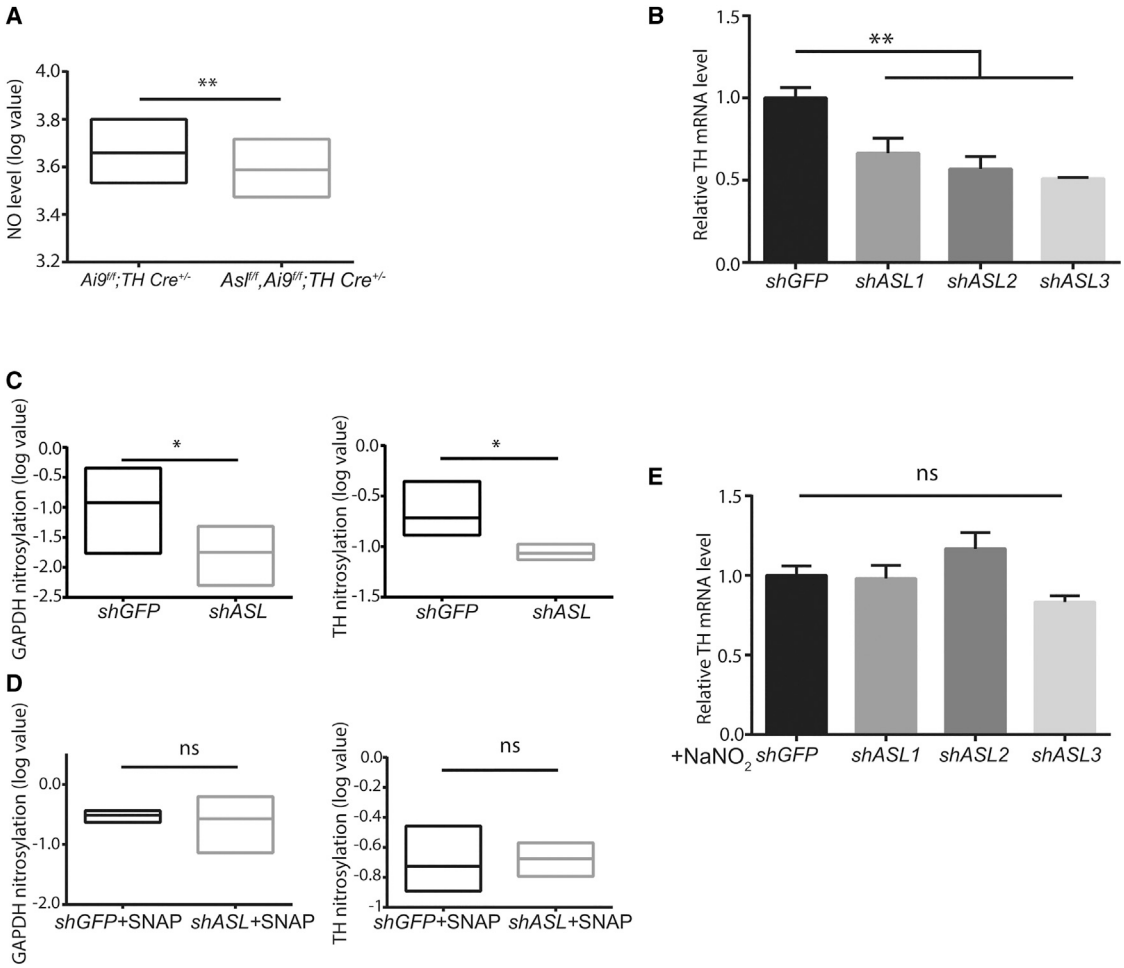

Figure 2. ASL Regulates TH Levels by Regulating NO Availability

(A) NO levels measurement using DAF-FM probe demonstrates significantly reduced NO levels in the LC of *Asl*$^{f/f}$*;Ai9*$^{f/f}$*;TH Cre*$^{+/-}$ mice as compared to *Ai9*$^{f/f}$*;TH Cre*$^{+/-}$ control mice (each experiment was performed with pair of control and *Asl*$^{f/f}$*;Ai9*$^{f/f}$*;TH Cre*$^{+/-}$ mice; n = 3).

(B) Knockdown of *ASL* in SH-SY5Y neurons using three different lentiviral *ASL-shRNA* clones associates with downregulation in *TH* mRNA levels.

(C) *shASL* SH-SY5Y neurons have significantly reduced nitrosylation of GAPDH (left) and of TH (right; measurement was performed ≥3 times).

(D) NO donors' supplementation to SH-SY5Y neurons rescues the differences in GAPDH (left) and TH (right) nitrosylation between *shASL* and *shGFP* control neurons.

(E) Treatment of *shASL* neurons with NO donors normalizes *TH* mRNA levels to that of *shGFP* control neurons (n ≥ 3; one-way ANOVA with Bonferroni).

Data represent mean ± SEM (*p < 0.05; **p < 0.01). See also Figure S3.

were significantly decreased, and its turnover rates were significantly upregulated in LC of *Asl*$^{f/f}$*;TH Cre*$^{+/-}$ in comparison to *Asl*$^{f/f}$ controls. Norepinephrine levels did not differ between *Asl*$^{f/f}$*;TH Cre*$^{+/-}$ and control mice following the stressful stimuli, likely because the majority of norepinephrine containing neural terminals are outside of the LC (Figure 3A). Indeed, the dependence of norepinephrine availability on ASL expression in the LC was clearly seen in the hippocampus, a target region for LC projections. During acute stress, significant elevations in norepinephrine levels were observed in the hippocampus in *Asl*$^{f/f}$ control, but not in *Asl*$^{f/f}$*;TH Cre*$^{+/-}$, mice (Figure 3B). Importantly, treatment with NO donors normalized norepinephrine levels in the LC (Figure 3C). Thus, noradrenergic transmission in *Asl*$^{f/f}$*;TH Cre*$^{+/-}$ mice facilitates NO-dependent reduced response in the LC.

LC-ASL cKO Neurons Have Impaired Firing Rate

The functional consequences of reduction in TH expression and in norepinephrine availability was further evaluated by recording LC neuronal activity in brainstem slices obtained from *Asl*$^{f/f}$ control and *Asl*$^{f/f}$*;TH Cre*$^{+/-}$ mice. We found that LC neurons in slices from *Asl*$^{f/f}$*;TH Cre*$^{+/-}$ mice demonstrate a spontaneous action potential firing activity that was more frequent when compared to *Asl*$^{f/f}$ control mice (Figures 4A–4C). The distributions of inter-spike intervals fitted with the normal gamma distribution (Figure 4B). Passive properties of LC neurons, as well as spike shape properties, were not significantly different between the groups, all except for the after-hyperpolarization recovery slope (Figures 4D–4F). We found the maximal slope to be significantly sharper in *Asl*$^{f/f}$*;TH Cre*$^{+/-}$ neurons than *Asl*$^{f/f}$ control. In *Asl*$^{f/f}$*;TH Cre*$^{+/-}$, this slope showed significant correlation with average

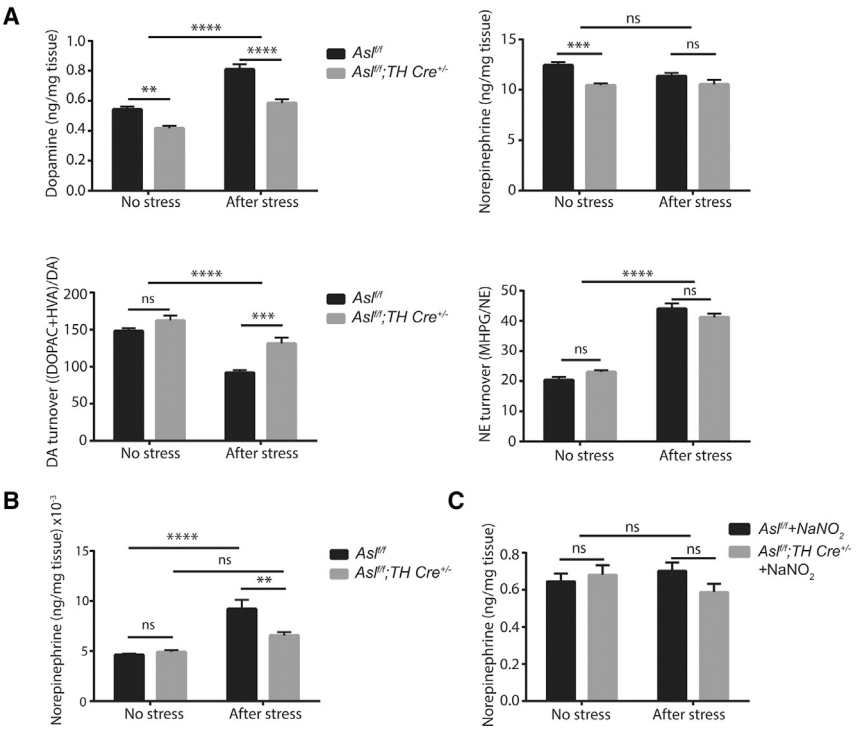

Figure 3. ASL Deficiency Associates with Decreased Catecholamine Synthesis

(A) Measurement of LC catecholamine levels show alterations in quantity and in turnover rates in both dopamine (left) and in norepinephrine (right), in $Asl^{f/f};TH\ Cre^{+/-}$ as compared to $Asl^{f/f}$ control mice ($n \geq 10$ mice in each group).

(B) Measurements of norepinephrine levels in the hippocampus following stress show decreased elevation in $Asl^{f/f};TH\ Cre^{+/-}$ as compared to $Asl^{f/f}$ control mice ($n \geq 9$ mice in each group).

(C) Measurements of LC norepinephrine levels of mice treated with $NaNO_2$ show no difference between $Asl^{f/f};TH\ Cre^{+/-}$ and $Asl^{f/f}$ control mice ($n \geq 5$ mice in each group).

Data represent mean ± SEM (non-repeated-measures two-way ANOVA with Bonferroni post hoc t tests; *p < 0.05; **p < 0.01; ***p < 0.001; ****p < 0.0001).

firing frequency, which links the spike shape properties to firing rate (Figures 4D–4F). Collectively, these results support that reduced TH activity following ASL loss alters neuronal function in the LC.

Phenotypic Consequences of ASL Deficiency in LC

Deregulation of LC has been strongly associated with attention problems in murine models as well as humans (Darcq and Kieffer, 2015; Janitzky et al., 2015; Kline et al., 2016; Tait et al., 2007). Thus, we first assessed whether individuals with ASLD are at risk for attention problem by using data from the Longitudinal Study of UCDs conducted by the Urea Cycle Disorders Consortium. From this dataset, we analyzed the parent- or participant-reported behavioral characteristics in individuals with ASLD in comparison to patients with argininosuccinate synthase deficiency (ASS1D), the urea cycle enzyme upstream of ASL. This analysis demonstrated that short attention span was reported at least during one study visit, in 55% of individuals with ASLD as compared to 39.4% with ASS1D (Figure S4A). As hyperammonemia can be a confounder for any behavioral outcomes in UCDs, we further evaluated the prevalence of self-reported short attention span in individuals who did not have any documented episodes of hyperammonemia. Even in the absence of documented hyperammonemia, 54% of individuals with ASLD reported short attention span, whereas the percentage in ASS1D was now 18% (Figure S4A). These provide a human context to the findings that some of the behavioral abnormalities in ASLD are due to cell-autonomous loss of ASL in the neurons. To validate these observations further, we compared attention problem scores on the Child Behavior Checklist (CBCL) reported in participants with ASLD and ASS1D using longitudinal quantile regression models. The standardized scores for the CBCL attention problems for individuals with ASLD and ASS1D were both within the pathological clinical range (i.e., decreased attention) when compared to the normative population (Figure S4B).

As LC is critically involved in orchestrating the central stress responses involving cardiovascular and stereotypical manifestations (Elam et al., 1984; Ogawa et al., 1977; Saran et al., 1978), we wanted to explore whether LC loss of ASL could contribute to the hypertension observed in mice and humans with ASLD. Using continuous blood pressure telemetric measurements, and consistent with our previous reports, we found that endothelial-ASL cKO mice ($Asl^{f/f};Cdn\ Cre^{+/-}$) have a significantly higher blood pressure (Kho et al., 2018). In contrast, LC-ASL cKO mice ($Asl^{f/f};TH\ Cre^{+/-}$) demonstrated blood pressure and heart rate that were comparable to their control littermates (Figures S4C and S4D). To evaluate whether loss of LC-ASL alters the hemodynamic responses to stress, we performed continued telemetry monitoring with the induction of acute psychological stress. As expected, immediately following the intruder stress, both $Asl^{f/f}$ control and $Asl^{f/f};TH\ Cre^{+/-}$ mice displayed an increase in blood pressure (Figure 5A). However, $Asl^{f/f};TH\ Cre^{+/-}$ mice had a three-fold increase in blood pressure levels as compared to controls (Figure 5A). Moreover, for 3 h following stress induction, $Asl^{f/f};TH\ Cre^{+/-}$ mice continued to have a higher blood pressure. Additionally, they required a longer recovery time to normalize blood pressure levels (Figures 5A and 5B). Interestingly, although the endothelial-ASL cKO mice have baseline hypertension, following stress induction their blood pressure elevation did not differ from that of $Asl^{f/f}$ control mice (Figure 5A).

To evaluate the effect ASL loss has on LC-related stereotypical behaviors, we examined the responses to restrain-stress stimuli in $Asl^{f/f};TH\ Cre^{+/-}$ mice by performing the open-field test. Although analysis of the locomotor activity parameters between genotypes showed no differences during non-stress state (Figure S4E), following acute stress exposure, $Asl^{f/f};TH$

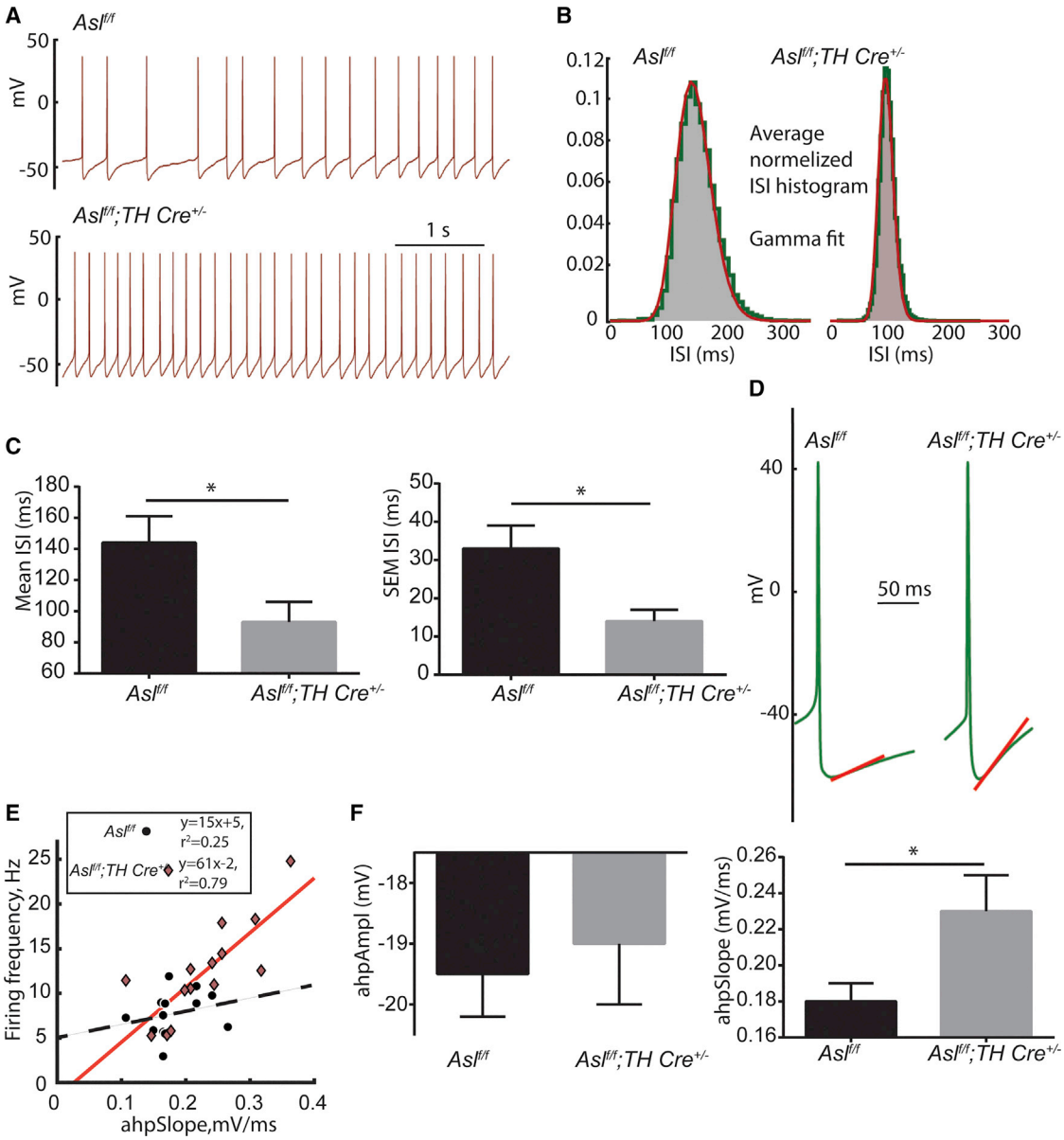

Figure 4. ASL Deficiency in the LC Associates with Increased Firing from LC Neurons

(A) Representative recordings of spontaneous action potentials of LC neurons. Upper panel —*Asl*$^{f/f}$ control, showing typical inter-spike interval variability; lower panel—*Asl*$^{f/f}$*;TH Cre*$^{+/-}$ (frequency 7.9 ± 0.6 Hz in *Asl*$^{f/f}$ control; 13.8 ± 2.0 Hz in *Asl*$^{f/f}$*;TH Cre*$^{+/-}$; $p < 0.01$).

(B) Averaged normalized inter-spike interval (ISI) histograms. (Left) *Asl*$^{f/f}$ control n = 14 is shown; (right) *Asl*$^{f/f}$*;TH Cre*$^{+/-}$ n = 15 cells are shown; red, gamma distribution probability density function fit with shape parameters 26 and 60 and scale parameters 5.9 and 1.7, respectively. ISI distributions from single recordings were also fit with gamma distribution (data not shown) with shape parameters 31 ± 6 and 122 ± 37 ($p < 0.03$) and scale parameters 8.4 ± 2.7 and 2.4 ± 0.8 ($p < 0.04$) in *Asl*$^{f/f}$ control and *Asl*$^{f/f}$*;TH Cre*$^{+/-}$, respectively.

(C) Spiking frequency presented as mean ISI (left; 144 ± 17 ms in *Asl*$^{f/f}$ control [n = 14 cells from 3 animals] and 93 ± 13 ms in *Asl*$^{f/f}$*;TH Cre*$^{+/-}$ [n = 15 cells from 3 animals] $p < 0.03$) and SEM. ISI as a measure of ISI variability (right; SEM ISI 33 ± 6 ms in *Asl*$^{f/f}$ control and 14 ± 3 ms in *Asl*$^{f/f}$*;TH Cre*$^{+/-}$; $p < 0.02$).

(D) Examples for averaged spike (first 10 spikes from a recording per cell), showing the "landmarks" used for analyzing the spike shape (red asterisks: spike threshold; spike peak; and after-hyperpolarization). Red line, AHP recovery slope.

(E) Firing frequency and after-hyperpolarization (AHP) recovery slope scatterplot and per-cell linear regression plot: Ct ● y = 15x + 5; r2 = 0.25; dashed line; cKO ◆ y = 61x − 2; r2 = 0.79; solid line.

(F) After hyperpolarization current properties; left to right, amplitude (ahpAmpl −19.5 ± 0.7 mV n = 13 and −19.0 ± 1.0 mV n = 14; n.s.) and recovery slope (ahpSlope 0.18 ± 0.01 mV/ms n = 13 and 0.23 ± 0.02 mV/ms n = 14; $p < 0.05$). In *Asl*$^{f/f}$*;TH Cre*$^{+/-}$ group, this slope is correlated with firing frequency (data not shown; correlation coefficient 0.79; $p < 0.001$; Pearson correlation), whereas in the *Asl*$^{f/f}$ control cells, this correlation was not observed (0.25; $p = 0.41$). Other

(legend continued on next page)

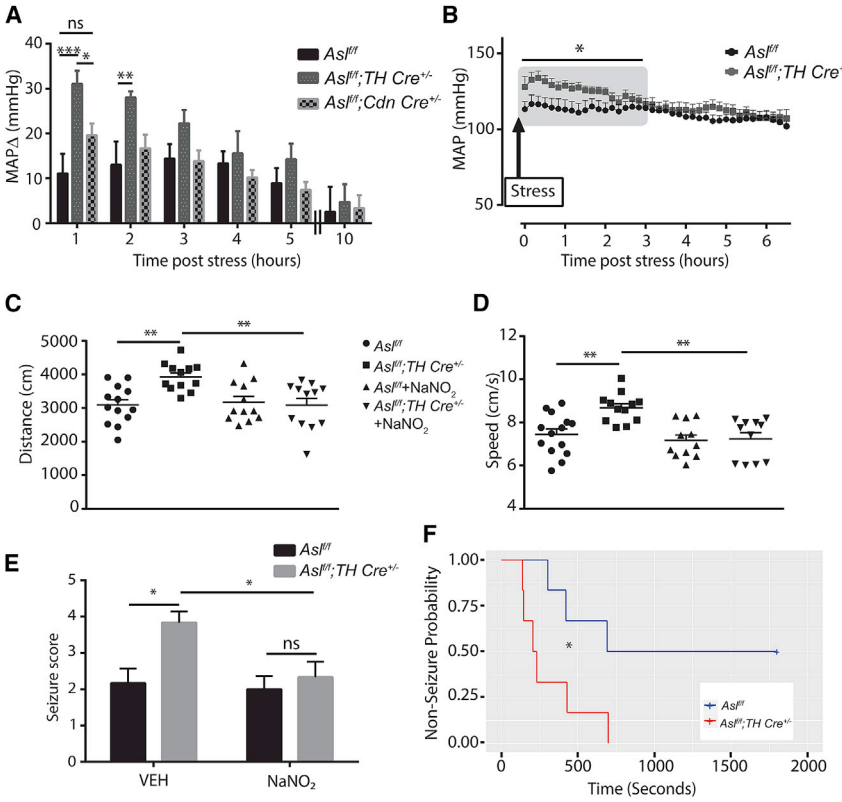

Figure 5. Phenotypic Consequences of ASL Deficiency in LC

(A) Measured mean arterial pressure (MAP) levels following induction of acute stress by exposure to intruder mice. The increase in blood pressure levels following stress is higher in *Asl*$^{f/f}$*;TH Cre*$^{+/-}$ mice and requires a longer recovery time as compared to *Asl*$^{f/f}$ control and to endothelial-ASL cKO mice ($n \geq 8$ in each group; repeated-measures two-way ANOVA with Holm-Sidak's post hoc t tests).

(B) Continuous blood pressure measurement during the first 3 h after stress induction demonstrates a significantly higher blood pressure in *Asl*$^{f/f}$*;TH Cre*$^{+/-}$ mice as compared to *Asl*$^{f/f}$ control mice ($n \geq 8$ in each group).

(C and D) Open-field test locomotor evaluation. Following stressful stimuli, *Asl*$^{f/f}$*;TH Cre*$^{+/-}$ mice present increase locomotor activity as indicated in distance (C) and speed (D), in comparison to *Asl*$^{f/f}$ control mice. Following treatment with NO donors, *Asl*$^{f/f}$*;TH Cre*$^{+/-}$ mice response to stressful stimuli is similar to that of *Asl*$^{f/f}$ control mice ($n \geq 11$ in each group; non-repeated-measures two-way ANOVA with Bonferroni post hoc t tests).

(E) Seizure score after injection of 50 mg/kg PTZ is higher in *Asl*$^{f/f}$*;TH Cre*$^{+/-}$ mice as compared to *Asl*$^{f/f}$ control mice. Following treatment with NO donor, there was no significant difference in the seizure reaction to injection between the two genotypes ($n = 6$ in each group).

(F) Kaplan Meier estimator presenting the probability of mice to develop myoclonic jerks from the time of PTZ injection. *Asl*$^{f/f}$*;TH Cre*$^{+/-}$ mice have more than 4-fold chance of developing myoclonic jerks as compared to *Asl*$^{f/f}$ control mice.

Data represent mean ± SEM (*$p < 0.05$; **$p < 0.01$; ***$p < 0.001$). See also Figure S4.

Cre$^{+/-}$ mice exhibited abnormal locomotor activity as reflected by increase in both distance traveled and speed (Figures 5C and 5D). Notably, analysis of the anxiety parameters between the groups showed no significant differences (Figure S4F).

Finally, patients with UCDs, including ASLD, have been reported to have an increased propensity to develop seizures (Baruteau et al., 2019; Huemer et al., 2016; Kölker et al., 2015a, 2015b). Because the LC region has a distinct antiepileptic effect in limiting both the spread and duration of seizures (Chachua et al., 2010; Fornai et al., 2011; Giorgi et al., 2003; Szot et al., 1999), we tested whether LC-ASL-cKO mice have high seizure sensitivity. By inducing seizures with pentylenetetrazol (PTZ) injections, we found that *Asl*$^{f/f}$*;TH Cre*$^{+/-}$ mice are significantly more reactive to PTZ-induced seizure as compared to *Asl*$^{f/f}$ control mice (Figure 5E). Furthermore, all *Asl*$^{f/f}$*;TH Cre*$^{+/-}$ mice developed myoclonic jerks with shorter latency as compared to only half of *Asl*$^{f/f}$ control mice (Figure 5F). Importantly, supplementing NO donors to *Asl*$^{f/f}$*;TH Cre*$^{+/-}$ mice rescued the LC stereotypical phenotypes of hyper-locomotion and seizure hypersensitivity, giving therapeutic context to our findings (Figures 5C–5E).

DISCUSSION

Behavioral abnormalities, attention deficit, seizures, and executive dysfunction are well-known manifestations in many subtypes of UCDs. Typically, these have been ascribed to injury caused by hyperammonemia, a classic phenotypic characteristic manifestation of UCDs. However, neuropsychological deficits have been observed in individuals with ASLD who have not experienced documented hyperammonemia. Thus, neuronal deficiency of arginine; neurotoxicity mediated by free radicals as well as by guanidinosuccinate, a metabolite that is generated from oxidation of argininosuccinate; and creatine deficiency have all been hypothesized as causative mechanisms (Baruteau et al., 2017, 2019).

Here, we demonstrate that, in the brain, ASL is prominently expressed in the LC, a highly important brain stem nucleus that has output projections of norepinephrine to multiple regions of the brain. Indeed, LC regulates attention-related functions, from learning and memory to stress. Consequently, LC dysfunction is associated with intellectual disabilities, ADHD-like behavior, seizures, motor problems, and hypertension. In several studies,

passive and active properties of LC neurons were not significantly different between the groups (data not shown; resting membrane potential −48.9 ± 0.7 mV n = 12 and −48.6 ± 0.9 mV n = 15; input resistance 113 ± 7 MOhm n = 13 and 121 ± 11 MOhm n = 15; spike threshold −39.8 ± 0.9 mV n = 12 and −38.6 ± 1.0 mV n = 15; spike amplitude 83.1 ± 2.2 mV n = 14 and 86.1 ± 2.5 mV n = 15; spike width 2.09 ± 0.08 ms n = 14 and 2.04 ± 0.06 ms n = 15 in *Asl*$^{f/f}$ control and *Asl*$^{f/f}$*;TH Cre*$^{+/-}$, respectively).

rare disorders enabled the dissection of consequences caused by a specific genetic alteration from the multiple changes that accompany complex diseases (Erez and DeBerardinis, 2015). Thus, the shared clinical manifestation between patients with ASLD and patients with LC dysfunction intrigued us to study the phenotypic consequences resulting from ASL deficiency in the LC.

Phenotypically, we found that LC loss of ASL in mice alters the stress response as manifested by a persistent locomotor activity and by high blood pressure and increases seizure sensitivity. The higher rates of LC discharges we demonstrate in ASL deficiency mice may result from loss of a local negative feedback of noradrenergic autoreceptors that regulate LC activity (Samuels and Szabadi, 2008). The increased activity of LC neurons may contribute to the enhanced motility of the LC-ASL-cKO mice in an open field, likely reflecting an exaggerated reaction to stressful stimuli. Indeed, a causal relationship has been demonstrated between LC firing and a general locomotor arousal (Carter et al., 2010). Importantly, we demonstrate that supplementation with NO donors rescue TH levels by increasing nitrosylation, thus normalizing norepinephrine levels. Subsequently, NO donors rescue both the seizure hyperactivity as well as the abnormal stress response.

Previous studies have shown that NO donors can penetrate the blood brain barrier (Gladwin et al., 2004; Nagababu et al., 2003). Our findings here demonstrating the beneficial response to NO donors in reaction to stressful stimuli are consistent with documented improvement in neurocognitive measures following treatment in a subject with ASLD (Nagamani et al., 2012a). Suggesting, that a better understanding of the role ASL plays in the LC will contribute to the management of ASLD patients and, more broadly, may shed light on the metabolic regulation of other more common LC-related pathologies.

STAR★METHODS

Detailed methods are provided in the online version of this paper and include the following:

- KEY RESOURCES TABLE
- LEAD CONTACT AND MATERIALS AVAILABILITY
- EXPERIMENTAL MODEL AND SUBJECT DETAILS
  - Human studies
  - In vivo animal studies
  - Cell cultures
- METHOD DETAILS
  - Transient transfection
  - Virus infection
  - Human subjects
  - Mice perfusion
  - NO treatment
  - Nitrosylation assay
  - Laser micro-dissection (LMD)
  - RNA sequencing
  - Library construction and sequencing
  - Sequence data analysis
  - Bioinformatics analysis
  - Telemetry probes implantation
  - Seizure Induction
  - Behavioral studies-open field test
  - Brain tissue biopsies collection
  - Catecholamine measurements
  - Immunostaining
  - Protein analysis: western blotting
  - RNA extraction and complementary DNA (cDNA) synthesis
  - *In situ* hybridization
  - Proteomic analysis
  - Flow cytometry for NO measurements
  - Electrophysiology
- QUANTIFICATION AND STATISTICAL ANALYSIS
- DATA AND CODE AVAILABILITY

SUPPLEMENTAL INFORMATION

Supplemental Information can be found online at https://doi.org/10.1016/j.celrep.2019.10.043.

CONSORTIA

We are grateful for the contributions of the Urea Cycle Disorders Consortium neuropsychologists—Fabienne Dietrich Alber, Talin Babikian, Heidi Bender, Christopher Boys, David Breiger, Corinna Buerger, Peter Burgard, Mina Nguyen-Driver, Benjamin Goodlett, Elizabeth Kerr, Casey Krueger, Eva Mamak, Jacqueline H. Sanz, David Schwartz, Susan Caudle (deceased, July 2017), Arianna Stefanos, Rachel Tangen, Magdalena Walter, Susan Waisbren, and Greta Wilkening.

ACKNOWLEDGMENTS

We are thankful for the intellectual discussions and inputs from Dr. Ofer Yizhar, Professor Gil Levkowitz, Dr. Yaniv Ziv, Dr. Matthias Prigge, and Professor Brendan Lee. We acknowledge and thank the Weizmann Institute for providing financial and infrastructural support. We greatly appreciate the support provided by the lab of Professor Alon Chen (Weizmann Institute Israel and Max Planck Institute of Psychiatry in Munich). We are thankful for the technical assistance we received from Dr. Ron Rotkop, Dr. Ayala Sharp, Dr. Edna Peleg, Ms. Sivan Galai, and Mr. Sharon Ovadia from the Weizmann Institute and Dr. Rotem Engelman from the lab of Professor Moran Benhar from the Technion. A.E. is incumbent of the Leah Omenn Career Development Chair and is supported by research grants from the European research program (ERC614204) and the Israel Science Foundation (ISF) (1343/13; 1952/13). A.E. received additional support from the Adelis Foundation, the Henry S. and Anne S. Reich Research Fund, the Dukler Fund for Cancer Research, the Paul Sparr Foundation, the Saul and Theresa Esman Foundation, Joseph Piko Baruch, and from the estate of Fannie Sherr. Y. Kuperman. is the incumbent of the Sarah and Rolando Uziel Research Associate Chair. M.T. is the incumbent of the Carolito Stiftung Research Fellow Chair in Neurodegenerative Diseases. The behavioral human data presented in the work were collected by the Urea Cycle Disorders Consortium (UCDC) (U54HD061221), a part of the NIH Rare Disease Clinical Research Network (RDCRN), supported through collaboration between the Office of Rare Diseases Research (ORDR), the National Center for Advancing Translational Science (NCATS), and the Eunice Kennedy Shriver National Institute of Child Health and Human Development (NICHD). The Urea Cycle Disorders Consortium is also supported by the O'Malley Foundation, the Rotenberg Family Fund, the Dietmar-Hopp Foundation, the Kettering Fund, and the National Urea Cycle Disorders Foundation.

AUTHOR CONTRIBUTIONS

S.L. performed most of the experiments described in the manuscript; E.A., T.M., and A.B. measured the catecholamine contents; S.V. from M.S. lab

performed the neuron firing analysis; R.E. helped with the immunostaining; Y. Kuperman, Y. Kuznetsov, and M.T. helped with the *in vivo* studies; R. Mazkereth helped with characterizing the phenotypes; R. McCarter from the UCDC performed the statistical analysis of the human data; S.C.S.N. provided us with the clinical data and analysis of ASLD patients as well as with crucial help with the writing of the manuscript; and M.S. and A.C. were highly involved in planning the relevant experiments and in the writing of the manuscript. A.E. initiated and led the study and wrote the manuscript. All authors were involved in discussions about study design and reviewed the manuscript.

DECLARATION OF INTERESTS

The authors declare no competing interests.

Received: July 2, 2019
Revised: September 18, 2019
Accepted: October 10, 2019
Published: November 19, 2019

REFERENCES

Anders, S., and Huber, W. (2010). Differential expression analysis for sequence count data. Genome Biol. *11*, R106.

Anders, S., Pyl, P.T., and Huber, W. (2015). HTSeq–a Python framework to work with high-throughput sequencing data. Bioinformatics *31*, 166–169.

Anderzhanova, E.A., Bächli, H., Buneeva, O.A., Narkevich, V.B., Medvedev, A.E., Thoeringer, C.K., Wotjak, C.T., and Kudrin, V.S. (2013). Strain differences in profiles of dopaminergic neurotransmission in the prefrontal cortex of the BALB/C vs. C57Bl/6 mice: consequences of stress and afobazole. Eur. J. Pharmacol. *708*, 95–104.

Baruteau, J., Jameson, E., Morris, A.A., Chakrapani, A., Santra, S., Vijay, S., Kocadag, H., Beesley, C.E., Grunewald, S., Murphy, E., et al. (2017). Expanding the phenotype in argininosuccinic aciduria: need for new therapies. J. Inherit. Metab. Dis. *40*, 357–368.

Baruteau, J., Perocheau, D.P., Hanley, J., Lorvellec, M., Rocha-Ferreira, E., Karda, R., Ng, J., Suff, N., Diaz, J.A., Rahim, A.A., et al. (2018). Argininosuccinic aciduria fosters neuronal nitrosative stress reversed by Asl gene transfer. Nat. Commun. *9*, 3505.

Baruteau, J., Diez-Fernandez, C., Lerner, S., Ranucci, G., Gissen, P., Dionisi-Vici, C., Nagamani, S., Erez, A., and Häberle, J. (2019). Argininosuccinic aciduria: recent pathophysiological insights and therapeutic prospects. J. Inherit. Metab. Dis. Published online February 5, 2019. https://doi.org/10.1002/jimd.12047.

Blecher-Gonen, R., Barnett-Itzhaki, Z., Jaitin, D., Amann-Zalcenstein, D., Lara-Astiaso, D., and Amit, I. (2013). High-throughput chromatin immunoprecipitation for genome-wide mapping of in vivo protein-DNA interactions and epigenomic states. Nat. Protoc. *8*, 539–554.

Braissant, O. (2004). Measurement of nitric oxide-related enzymes in the brain by in situ hybridization. Methods Mol. Biol. *279*, 113–124.

Bredt, D.S., Hwang, P.M., and Snyder, S.H. (1990). Localization of nitric oxide synthase indicating a neural role for nitric oxide. Nature *347*, 768–770.

Brunetti-Pierri, N., Erez, A., Shchelochkov, O., Craigen, W., and Lee, B. (2009). Systemic hypertension in two patients with ASL deficiency: a result of nitric oxide deficiency? Mol. Genet. Metab. *98*, 195–197.

Calabrese, V., Mancuso, C., Calvani, M., Rizzarelli, E., Butterfield, D.A., and Stella, A.M. (2007). Nitric oxide in the central nervous system: neuroprotection versus neurotoxicity. Nat. Rev. Neurosci. *8*, 766–775.

Carter, M.E., Yizhar, O., Chikahisa, S., Nguyen, H., Adamantidis, A., Nishino, S., Deisseroth, K., and de Lecea, L. (2010). Tuning arousal with optogenetic modulation of locus coeruleus neurons. Nat. Neurosci. *13*, 1526–1533.

Chachua, T., Bilanishvili, I., Khizanishvili, N., and Nanobashvili, Z. (2010). Noradrenergic modulation of seizure activity. Georgian Med. News, 34–39.

Darcq, E., and Kieffer, B.L. (2015). PI3K signaling in the locus coeruleus: a new molecular pathway for ADHD research. EMBO Mol. Med. *7*, 859–861.

Elam, M., Yao, T., Svensson, T.H., and Thoren, P. (1984). Regulation of locus coeruleus neurons and splanchnic, sympathetic nerves by cardiovascular afferents. Brain Res. *290*, 281–287.

Erez, A., and DeBerardinis, R.J. (2015). Metabolic dysregulation in monogenic disorders and cancer - finding method in madness. Nat. Rev. Cancer *15*, 440–448.

Erez, A., Nagamani, S.C., and Lee, B. (2011a). Argininosuccinate lyase deficiency-argininosuccinic aciduria and beyond. Am. J. Med. Genet. C. Semin. Med. Genet. *157C*, 45–53.

Erez, A., Nagamani, S.C., Shchelochkov, O.A., Premkumar, M.H., Campeau, P.M., Chen, Y., Garg, H.K., Li, L., Mian, A., Bertin, T.K., et al. (2011b). Requirement of argininosuccinate lyase for systemic nitric oxide production. Nat. Med. *17*, 1619–1626.

Feodorova, Y., Koch, M., Bultman, S., Michalakis, S., and Solovei, I. (2015). Quick and reliable method for retina dissociation and separation of rod photoreceptor perikarya from adult mice. MethodsX *2*, 39–46.

Ficicioglu, C., Mandell, R., and Shih, V.E. (2009). Argininosuccinate lyase deficiency: longterm outcome of 13 patients detected by newborn screening. Mol. Genet. Metab. *98*, 273–277.

Fornai, F., Ruffoli, R., Giorgi, F.S., and Paparelli, A. (2011). The role of locus coeruleus in the antiepileptic activity induced by vagus nerve stimulation. Eur. J. Neurosci. *33*, 2169–2178.

Forrester, M.T., Thompson, J.W., Foster, M.W., Nogueira, L., Moseley, M.A., and Stamler, J.S. (2009). Proteomic analysis of S-nitrosylation and denitrosylation by resin-assisted capture. Nat. Biotechnol. *27*, 557–559.

Foster, M.W., Hess, D.T., and Stamler, J.S. (2009). Protein S-nitrosylation in health and disease: a current perspective. Trends Mol. Med. *15*, 391–404.

Giorgi, F.S., Ferrucci, M., Lazzeri, G., Pizzanelli, C., Lenzi, P., Alessandrl, M.G., Murri, L., and Fornai, F. (2003). A damage to locus coeruleus neurons converts sporadic seizures into self-sustaining limbic status epilepticus. Eur. J. Neurosci. *17*, 2593–2601.

Gladwin, M.T., Crawford, J.H., and Patel, R.P. (2004). The biochemistry of nitric oxide, nitrite, and hemoglobin: role in blood flow regulation. Free Radic. Biol. Med. *36*, 707–717.

Guix, F.X., Uribesalgo, I., Coma, M., and Muñoz, F.J. (2005). The physiology and pathophysiology of nitric oxide in the brain. Prog. Neurobiol. *76*, 126–152.

Harraz, M.M., and Snyder, S.H. (2015). Nitric oxide-GAPDH transcriptional signaling mediates behavioral actions of cocaine. CNS Neurol. Disord. Drug Targets *14*, 757–763.

Huemer, M., Carvalho, D.R., Brum, J.M., Ünal, Ö., Coskun, T., Weisfeld-Adams, J.D., Schrager, N.L., Scholl-Bürgi, S., Schlune, A., Donner, M.G., et al. (2016). Clinical phenotype, biochemical profile, and treatment in 19 patients with arginase 1 deficiency. J. Inherit. Metab. Dis. *39*, 331–340.

Huetteman, D.A., and Bogie, H. (2009). Direct blood pressure monitoring in laboratory rodents via implantable radio telemetry. Methods Mol. Biol. *573*, 57–73.

Janitzky, K., Lippert, M.T., Engelhorn, A., Tegtmeier, J., Goldschmidt, J., Heinze, H.J., and Ohl, F.W. (2015). Optogenetic silencing of locus coeruleus activity in mice impairs cognitive flexibility in an attentional set-shifting task. Front. Behav. Neurosci. *9*, 286.

Kho, J., Tian, X., Wong, W.T., Bertin, T., Jiang, M.M., Chen, S., Jin, Z., Shchelochkov, O.A., Burrage, L.C., Reddy, A.K., et al. (2018). Argininosuccinate lyase deficiency causes an endothelial-dependent form of hypertension. Am. J. Hum. Genet. *103*, 276–287.

Kim, D., Pertea, G., Trapnell, C., Pimentel, H., Kelley, R., and Salzberg, S.L. (2013). TopHat2: accurate alignment of transcriptomes in the presence of insertions, deletions and gene fusions. Genome Biol. *14*, R36.

Kleijer, W.J., Garritsen, V.H., Linnebank, M., Mooyer, P., Huijmans, J.G., Mustonen, A., Simola, K.O., Arslan-Kirchner, M., Battini, R., Briones, P., et al. (2002). Clinical, enzymatic, and molecular genetic characterization of a biochemical variant type of argininosuccinic aciduria: prenatal and postnatal diagnosis in five unrelated families. J. Inherit. Metab. Dis. *25*, 399–410.

Kline, R.L., Zhang, S., Farr, O.M., Hu, S., Zaborszky, L., Samanez-Larkin, G.R., and Li, C.S. (2016). The effects of methylphenidate on resting-state functional connectivity of the basal nucleus of meynert, locus coeruleus, and ventral tegmental area in healthy adults. Front. Hum. Neurosci. *10*, 149.

Kölker, S., Garcia-Cazorla, A., Valayannopoulos, V., Lund, A.M., Burlina, A.B., Sykut-Cegielska, J., Wijburg, F.A., Teles, E.L., Zeman, J., Dionisi-Vici, C., et al. (2015a). The phenotypic spectrum of organic acidurias and urea cycle disorders. Part 1: the initial presentation. J. Inherit. Metab. Dis. *38*, 1041–1057.

Kölker, S., Valayannopoulos, V., Burlina, A.B., Sykut-Cegielska, J., Wijburg, F.A., Teles, E.L., Zeman, J., Dionisi-Vici, C., Barić, I., Karall, D., et al. (2015b). The phenotypic spectrum of organic acidurias and urea cycle disorders. Part 2: the evolving clinical phenotype. J. Inherit. Metab. Dis. *38*, 1059–1074.

Korosi, A., Veening, J.G., Kozicz, T., Henckens, M., Dederen, J., Groenink, L., van der Gugten, J., Olivier, B., and Roubos, E.W. (2006). Distribution and expression of CRF receptor 1 and 2 mRNAs in the CRF over-expressing mouse brain. Brain Res. *1072*, 46–54.

Kovalevich, J., and Langford, D. (2013). Considerations for the use of SH-SY5Y neuroblastoma cells in neurobiology. Methods Mol. Biol. *1078*, 9–21.

Lågas, P.A., and Ruokonen, A. (1991). Late onset argininosuccinic aciduria in a paranoid retardate. Biol. Psychiatry *30*, 1229–1232.

Madisen, L., Zwingman, T.A., Sunkin, S.M., Oh, S.W., Zariwala, H.A., Gu, H., Ng, L.L., Palmiter, R.D., Hawrylycz, M.J., Jones, A.R., et al. (2010). A robust and high-throughput Cre reporting and characterization system for the whole mouse brain. Nat. Neurosci. *13*, 133–140.

McCall, J.G., Al-Hasani, R., Siuda, E.R., Hong, D.Y., Norris, A.J., Ford, C.P., and Bruchas, M.R. (2015). CRH engagement of the locus coeruleus noradrenergic system mediates stress-induced anxiety. Neuron *87*, 605–620.

Mercimek-Mahmutoglu, S., Moeslinger, D., Häberle, J., Engel, K., Herle, M., Strobl, M.W., Scheibenreiter, S., Muehl, A., and Stöckler-Ipsiroglu, S. (2010). Long-term outcome of patients with argininosuccinate lyase deficiency diagnosed by newborn screening in Austria. Mol. Genet. Metab. *100*, 24–28.

Mori, M., and Gotoh, T. (2004). Arginine metabolic enzymes, nitric oxide and infection. J. Nutr. *134* (*10, Suppl*), 2820S–2825S, discussion 2853S.

Nagababu, E., Ramasamy, S., Abernethy, D.R., and Rifkind, J.M. (2003). Active nitric oxide produced in the red cell under hypoxic conditions by deoxyhemoglobin-mediated nitrite reduction. J. Biol. Chem. *278*, 46349–46356.

Nagamani, S.C.S., Erez, A., and Lee, B. (2011). Argininosuccinate lyase deficiency. In GeneReviews, *Volume R*, M.P. Adam, H.H. Ardinger, R.A. Pagon, S.E. Wallace, L.J.H. Bean, K. Stephens, and A. Amemiya, eds. (University of Washington).

Nagamani, S.C., Campeau, P.M., Shchelochkov, O.A., Premkumar, M.H., Guse, K., Brunetti-Pierri, N., Chen, Y., Sun, Q., Tang, Y., Palmer, D., et al. (2012a). Nitric-oxide supplementation for treatment of long-term complications in argininosuccinic aciduria. Am. J. Hum. Genet. *90*, 836–846.

Nagamani, S.C., Erez, A., and Lee, B. (2012b). Argininosuccinate lyase deficiency. Genet. Med. *14*, 501–507.

Ogawa, M., Fujita, Y., Niwa, M., Takami, N., and Ozaki, M. (1977). Role on blood pressure regulation of noradrenergic neurons originating from the locus coeruleus in the Kyoto-Wistar rat [proceedings]. Jpn. Heart J. *18*, 586–587.

Paxinos, G., and Franklin, K.B.J. (2001). The Mouse Brain in Stereotaxic Coordinates, 2nd Edition (San Diego: Academic Press).

Samuels, E.R., and Szabadi, E. (2008). Functional neuroanatomy of the noradrenergic locus coeruleus: its roles in the regulation of arousal and autonomic function part I: principles of functional organisation. Curr. Neuropharmacol. *6*, 235–253.

Sanchez-Padilla, J., Guzman, J.N., Ilijic, E., Kondapalli, J., Galtieri, D.J., Yang, B., Schieber, S., Oertel, W., Wokosin, D., Schumacker, P.T., and Surmeier, D.J. (2014). Mitochondrial oxidant stress in locus coeruleus is regulated by activity and nitric oxide synthase. Nat. Neurosci. *17*, 832–840.

Saran, R.K., Sahuja, R.C., Gupta, N.N., Hasan, M., Bhargava, K.P., Shanker, K., and Kishor, K. (1978). 3-Methoxy-4-hydroxyphenylglycol in cerebrospinal fluid and vanillylmandelic acid in urine of humans with hypertension. Science *200*, 317–318.

Szot, P., Weinshenker, D., White, S.S., Robbins, C.A., Rust, N.C., Schwartzkroin, P.A., and Palmiter, R.D. (1999). Norepinephrine-deficient mice have increased susceptibility to seizure-inducing stimuli. J. Neurosci. *19*, 10985–10992.

Tait, D.S., Brown, V.J., Farovik, A., Theobald, D.E., Dalley, J.W., and Robbins, T.W. (2007). Lesions of the dorsal noradrenergic bundle impair attentional set-shifting in the rat. Eur. J. Neurosci. *25*, 3719–3724.

Tekin, I., Roskoski, R., Jr., Carkaci-Salli, N., and Vrana, K.E. (2014). Complex molecular regulation of tyrosine hydroxylase. J. Neural Transm. (Vienna) *121*, 1451–1481.

Tuchman, M., McCullough, B.A., and Yudkoff, M. (2000). The molecular basis of ornithine transcarbamylase deficiency. Eur. J. Pediatr. *159* (*Suppl 3*), S196–S198.

Tuchman, M., Lee, B., Lichter-Konecki, U., Summar, M.L., Yudkoff, M., Cederbaum, S.D., Kerr, D.S., Diaz, G.A., Seashore, M.R., Lee, H.S., et al.; Urea Cycle Disorders Consortium of the Rare Diseases Clinical Research Network (2008). Cross-sectional multicenter study of patients with urea cycle disorders in the United States. Mol. Genet. Metab. *94*, 397–402.

Volk, N., Pape, J.C., Engel, M., Zannas, A.S., Cattane, N., Cattaneo, A., Binder, E.B., and Chen, A. (2016). Amygdalar microRNA-15a is essential for coping with chronic stress. Cell Rep. *17*, 1882–1891.

Wang, Y., Sung, C.C., and Chung, K.K. (2017). Novel enhancement mechanism of tyrosine hydroxylase enzymatic activity by nitric oxide through S-nitrosylation. Sci. Rep. *7*, 44154.

Westmark, C.J., Westmark, P.R., Beard, A.M., Hildebrandt, S.M., and Malter, J.S. (2008). Seizure susceptibility and mortality in mice that over-express amyloid precursor protein. Int. J. Clin. Exp. Pathol. *1*, 157–168.

Xu, Z.Q., Pieribone, V.A., Zhang, X., Grillner, S., and Hökfelt, T. (1994). A functional role for nitric oxide in locus coeruleus: immunohistochemical and electrophysiological studies. Exp. Brain Res. *98*, 75–83.

Xu, R., Serritella, A.V., Sen, T., Farook, J.M., Sedlak, T.W., Baraban, J., Snyder, S.H., and Sen, N. (2013). Behavioral effects of cocaine mediated by nitric oxide-GAPDH transcriptional signaling. Neuron *78*, 623–630.

STAR★METHODS

KEY RESOURCES TABLE

REAGENT or RESOURCE	SOURCE	IDENTIFIER
Antibodies		
Rabbit polyclonal anti-ASL	Abcam	Cat# ab97370; RRID:AB_10680261
Sheep polyclonal anti-TH	Merckmillipore	Cat# AB1542; RRID:AB_90755
Rabbit polyclonal anti-TH	Cell Signaling	Cat# 2792; RRID:AB_2303165
Mouse monoclonal anti-GAPDH	Abcam	Cat# ab8245; RRID:AB_2107448
Rabbit monoclonal anti-GAPDH	Cell Signaling	2118; RRID:AB_561053
Bacterial and Virus Strains		
Lentiviral pLKO.1 ASL shRNA target gene set	Dharmacon	RHS4533
Biological Samples		
Human brain tissue array	Biomax	Nct17N002A48
Chemicals, Peptides, and Recombinant Proteins		
Puromycin	Sigma-Aldrich	P8833
RIPA	Sigma-Aldrich	R0278
Protease inhibitor cocktail	Calbiochem	539131
Opti-MEM® I Reduced Serum Medium	ThermoFisher Scientific	11058021
Sodium Nitrlte $NaNO_2$	Sigma-Aldrich	S2252
S-Nitroso-N-acetyl-DL-penicillamine (SNAP)	CayMan chemicals	Cat# 82250
Alltrans-retinoic acid	Sigma-Aldrich	R2625
12-O-tetradecanoylphorbol 13-acetate	Sigma-Aldrich	P8139
Critical Commercial Assays		
RNeasy Mini Kit	QIAGEN	74104
RNase-Free DNase Set	QIAGEN	79254
SYBR green PCR master mix	Thermo Fisher scientific	4385612
BCA Protein Assay Kit	ThermoFisher Scientific	23225
Purelink RNA micro kit	ThermoFisher Scientific	12183016
Viral packaging mix	Renium	K4975-00
Deposited Data		
RNA-seq	This paper	GSE138471
Experimental Models: Cell Lines		
SH-SY5Y	ATTC	CRL-2266
Experimental Models: Organisms/Strains		
Mouse: C57BL/6JOlaHsd	Envigo	N/A
Mouse: B6.FVB-Tg(Cdh5-cre)7Mlia/J	The Jackson Laboratory	Stock No: 006137
Mouse: B6.Cg-Tg(Th-cre)1Tmd/J	Laboratory of Dr. Ofer Yizhar	N/A
Mouse: dTomato	Laboratory of Prof. Alon Chen	(Madisen et al., 2010)
Oligonucleotides		
Human_HPRT_qPCR _F ATTGACACTGGCAAAACAATGC	This paper	N/A
Human_HPRT_qPCR _R TCCAACACTTCGTGGGGTCC	This paper	N/A
Human_ASL_qPCR _F ATGGCCTCGGAGAGTGGGAA	This paper	N/A
Human_ASL_qPCR _R GCTTTGCTGCCTTGAACATCCA	This paper	N/A

(*Continued on next page*)

Continued

REAGENT or RESOURCE	SOURCE	IDENTIFIER
Human_TH_qPCR _F	This paper	N/A
TGTCCACGCTGTACTGGTTC		
Human_TH_qPCR _R	This paper	N/A
CACCATAGGCCTTCACCTCC		
Human_cFOS_qPCR _F	This paper	N/A
CTGATACACTCCAAGCGGAGA		
Human_cFOS_qPCR _R	This paper	N/A
TTGGCAATCTCGGTCTGCAA		
Human_VGF_qPCR _F	This paper	N/A
TCCCGATCTTCCCCTGTCC		
Human_VGF_qPCR _R	This paper	N/A
GCCGGAGACAGCTGGTG		
Mouse_HPRT_qPCR _F	This paper	N/A
GCAGTACAGCCCCAAAATGG		
Mouse_HPRT_qPCR _R	This paper	N/A
GGTTCCTTTTCACCAGCAAGCT		
Mouse_ActB_qPCR _F	This paper	N/A
CTGTCCCTGTATGCCTCTG		
Mouse_ ActB _qPCR _R	This paper	N/A
ATGTCACGCACGATTTCC		
Mouse_Asl_qPCR _F	This paper	N/A
GAAGGAACTCATCGGTGAAGCT		
Mouse_ Asl_qPCR _R	This paper	N/A
CCTCATCCACAGCCTGAGGT		
Mouse_ TH _qPCR _F	This paper	N/A
AATACAAGCAGGGTGAGCCA		
Mouse_ TH _qPCR _R	This paper	N/A
CTTCAGCGTGGCCTATACCT		
Forward primer for Asl *in situ* hybridization tgcagggaagctacacacag	This paper	N/A
Reverse primer for Asl *in situ* hybridization ttaggtcctctgccatcctg	This paper	N/A
ActB: Mm00607939_s1	ThermoFisher Scientific	Cat# 4331182
Asl: Mm01197741_m1	ThermoFisher Scientific	Cat# 4448892
Th: Mm00447557_m1	ThermoFisher Scientific	Cat# 4331182
Software and Algorithms		
ImageJ		https://fiji.sc/
Ingenuity Pathways Analysis	Ingenuity® Systems	https://www.ingenuity.com
Prism	GraphPad Software	https://www.graphpad.com/scientific-software/prism/

LEAD CONTACT AND MATERIALS AVAILABILITY

Further information and requests for resources and reagents should be directed to and will be fulfilled by the Lead Contact, Ayelet Erez (ayelet.erez@weizmann.ac.il).

This study did not generate new reagents.

EXPERIMENTAL MODEL AND SUBJECT DETAILS

Human studies

The Longitudinal Study of UCDs is an observational natural history study being conducted by the NIH Rare Disease Clinical Research Network's Urea Cycle Disorders Consortium (UCDC). The study, now in its 13th year is conducted at 14 sites in the United States, Canada, Germany, and Switzerland. Clinical, laboratory, patient-reported, and neuropsychological data are collected systematically across all sites according to guidelines outlined in a manual of operations. Informed consent is obtained from all participants prior to enrollment. The study is monitored by an independent data safety monitoring board of the Eunice Kennedy Shriver National Institute of Child Health and Human Development. From this study, we analyzed two sets of data. CNMC protocol number - Pro00000161 – Longitudinal Study of Urea Cycle Disorders. The first study was the parent- or participant-reported behavioral characteristics in individuals with ASLD and ASS1D. A total of 100 individuals with ASLD (median age 10.9 years, IQR 5.3-21) and 89 individuals with ASS1D (median age 10.2 years, IQR 5.5-16.24) who were enrolled in the study were included in the analyses. The second was attention scores for the CBCL which was administered by certified neuropsychologists or psychological associates. The attention scores from the CBCL were converted to a standardized score where 100 represents the population mean and scores below 85 and above 115 are considered clinically significant. The formulae used for conversion to standardized scores are as follows: for z-score, SS = (z*15)+100; for scaled scores, Z = (ScS-10)/3 and SS = (z*15)+100; for T-scores, z = (T-50)/10 and SS = (z*15)+100. Using longitudinal data, we implemented multiple quantile regression models, accounting for the correlation across multiple assessments per subject, to compare the median scores on CBCL attention scores in individuals with ASLD and ASS1D. At assessment points, the models controlled for the frequency of prior hyperammonemic events, prior incidents of coma or instances of increased intracranial pressure, as well as the peak ammonia level, the maximum length of stay and the current BRIEF Global Executive Composite (GEC) score. Subgroup analysis focused on comparing the same outcomes in individuals with ASLD and ASS1D who never experienced a hyperammonemic event controlling only for the current BRIEF GEC score. All outcomes were represented as standard scores normed to a mean of 100 and a standard deviation of 15. In the study cohort included, for ASLD, 50.00% (63 subjects) were female, 46.83% (59 subjects) were male, and 3.17% (4 subjects) unknown. For ASS1D, 53.98% (61 subjects) were female, 39.82% (45 subjects) were male, and 6.19% (7 subjects) were unknown. These are not different from expected distributions thus there was no bias in any gender selection

In vivo animal studies

All animal procedures were approved by the Institutional Animal Care and Use Committee (applications number: 07201118-1) and were performed in strict adherence to Weizmann Institute Animal Care and Use guidelines. Mice were purchased from Jackson Laboratory (Bar Harbor, ME, USA). B6.FVB-Tg(Cdh5-cre)7Mlia/J. C57BL/6JOlaHsd mice were purchased from ENVIGO RMS (ISRAEL). The B6.Cg-Tg(Th-cre)1Tmd/J and tdTomato mice were kindly given to us by Dr. Ofer Yizhar and Professor Alon Chen respectively (Madisen et al., 2010). Mice were monitored daily by Weizmann Institute staff and veterinary personnel for health and activity. Mice were given *ad libitum* access to water and standard mouse chow with 12-hr light/dark cycles. For the blood pressure experiment of Cdh5-cre mice, animals received arginine free diet (Envigo,TD09152 TEKLAD) from weaning. Experiments were conducted on 8-15-week-old male mice during the dark phase. For the flow cytometry experiments, cells were taken from 20-25 days old mice. Littermates of age and gender matched mice were randomly assigned to experimental groups.

Cell cultures

SH-SY5Y human neuroblastoma cells (American Type Culture Collection, ATCC, Manassas, VA, USA) were grown in DMEM (Dulbecco's modified Eagle's medium) supplemented with 10% heat-inactivated FBS, 100 units/mL streptomycin, and 100 μg/mL penicillin at 37°C in a humidified 5% CO2 atmosphere. All cells were tested routinely for mycoplasma using a Mycoplasma EZ-PCR test kit (20–700-20, Biological Industries). The cells were differentiated by treatment with Alltrans-retinoic acid (R2625 Sigma) 0.01M 2 and 4 days after plating, followed by treatment with 80 nM 12-O-tetradecanoylphorbol 13-acetate (TPA, P8139 Sigma), 6 and 8 day after plating.

METHOD DETAILS

Transient transfection

SH-SY5Y cells were seeded in 6-well plates at 200,000 cells/well. At the following day, cells were transfected with 3μg of either control vector (*shGFP*) or siRNA targeted to *ASL* (*shASL*) mRNA (TAMAR laboratory RHS4533). Transfection was done using Lipofectamine® 2000 Reagent (Catalog #: 11668-019, Invitrogen) in the presence of Opti-MEM® I Reduced Serum Medium (Catalog #: 31985-062, Invitrogen). 4 hours after transfection, medium was replaced, and experiments were performed starting 48 hours post transfection.

Virus infection

HEK293T cells were used to package the lentivirus. HEK293T cells in the logarithmic growth phase were seeded into a 10cm plate. Once cell confluence reached 80%, viral packaging mix (Renium K4975-00) and1μg of either *shGFP* or *shASL* were co-transfected

into HEK293T cells with the aid of lipofectamine 2000. 48 h after transfection, the supernatant of HEK293T cells was collected and centrifuged (1000 rpm) at 4°C for 10 min to remove cell debris. SH-SY5Ycells were seeded in 6-well plates (200,000 cells/well) and grown to reach approximately 80% confluency. 0.5ml of the supernatant was added to the cell culture medium without Penicillin-Streptomycin and incubated with the cells for 12 h. In the next day, the medium was replaced by fresh medium. The cells were then transferred to 10cm plate and Puromycin (4 μg/mL) was added for 4 days.

Human subjects

Brain tissue arrays were obtained from US BIOMAX, tissue ID: Nct17N002A48.

Mice perfusion

Following euthanasia, mice were rapidly perfused with cold 4% PFA in PBS. Mice brains were rapidly removed, immersed in freshly 4% paraformaldehyde for 24 hours, and then transmitted to 1% paraformaldehyde for 24 hours. For *in situ* hybridization mice brains were placed in 1 × PBS with 30% sucrose for another 24 hours and then frozen and sectioned in coronal plane using a microtome. For immunostaining, mouse brains were embedded in paraffin.

NO treatment

For *in vitro* assays, either 100 μM S-Nitroso-N-acetyl-DL-penicillamine (SNAP) (CayMan chemicals 82250) was added to the medium 5 minutes before cell collection, or Sodium Nitrite ($NaNO_2$) 10mM was added 10 hours before collection. For *in vivo* rescue experiments, mice were treated with $NaNO_2$ 100mg/kg in drinking water, renewed every 3 days (Sigma-Aldrich, St. Louis, MO, catalog number S2252).

Nitrosylation assay

Detection of protein nitrosylation was performed using the SNO-RAC method (Forrester et al., 2009) with minor adjustments. Briefly, cell lysates were prepared, and a total of ~2 mg protein was used for each experimental condition. The blocking step was performed for 30 min at 50°C, in the presence of 40 mM N-Ethylmaleimide (NEM) with frequent vortexing. After the acetone precipitation step, proteins were recovered by centrifugation at 2000 g for 5 min at 4°C, and the pellets were resuspended in HENS buffer (100 mM HEPES, 1 mM EDTA, 0.1 mM neocuproine, 1% SDS, pH 7.5). This material was added to 100 μL thiopropyl Sepharose beads (GE Healthcare) in the presence of 50 mM sodium ascorbate. Following rotation in the dark overnight at 4°C, the beads were washed with 4 × 1 mL HENS buffer, then 2 × 1 mL HENS/10 buffer (HENS diluted 1:10). Captured proteins were eluted with 30 μL HENS/10 containing 250 mM 2-mercaptoethanol for 20 min at room temperature and analyzed by western blotting.

Laser micro-dissection (LMD)

Brain were removed rapidly, briefly washed in cold PBS, embedded and frozen in OCT on dry ice without fixation. 8 μm thick sections were cut from the frozen block, mounted on polyethylene membrane-coated glass slides (Zeiss, A4151909081000), air-dried for 1 m at room temperature and put in −80°C. At the day of the experiment, slides were thawed for 5 minutes in room temperature followed by fixation in 70% ethanol (30 s), incubation in DEPC water, stained with 150μl 1% crystal violet acetate solution (Sigma-Aldrich C5042), and washed vigorously in 100% ethanol for a total of 30 s and air-dried for 3 minutes before microdissection. Tissue sections were microdissected using a UV laser-based PALM Microbeam (Zeiss). The cutting was performed with the following parameters: PALM 40X lens, cut energy 35 (1-100), cut focus 65 (1-100). Tissue fragments were catapulted and collected in 0.2ml adhesive cap tubes (Zeiss, A4151909181000) with these settings: LPC energy 50 (1-100), LPC focus 63 (1-100). The capturing success was visually confirmed by focusing the PALM on the targeted adhesive cap after the collection session. 100 cells were selected for microdissection from the LC of each mouse. Samples from LMD were used for RNA sequencing, RT-PCR and proteomic analysis. For TaqMan probes analysis, RNA was extracted using PureLink RNA Micro Scale Kit (ThermosFisher).

RNA sequencing

Samples of 100 lysed cells were amplified separately using SMARTSeq Ultra Low Input RNA V4 kit from (Clontech 634890). After the amplification step (16 cycles), the amplicons were fragmented to fragment sizes of about 300bp using Covaris E220 (Covaris,Inc.,Woburn, MA, USA). The amplified fragments were processed to libraries according to the chip seq protocol as previously described (Blecher-Gonen et al., 2013). Libraries were evaluated by Qubit and TapeStation. Sequencing libraries were constructed with barcodes to allow multiplexing of all samples in one lane. Between 17-20.5 million single-end 60-bp reads were sequenced per sample using Illumina HiSeq 2500 V4 instrument.

Library construction and sequencing

Total RNA for each sample, was processed using the SMARTer Ultra Low Input RNA, followed by in-house DNA Seq protocol. Sequencing Libraries were constructed with barcodes to allow multiplexing of 12 samples on 1 lane of Illumina HiSeq machine, using the Single-Read 60 protocol (v4). The output was ~18.6 million reads per sample. Fastq files for each sample were generated with bcl2fastq-v2.17.1.14.

Sequence data analysis

Poly-A/T stretches and Illumina adapters were trimmed from the reads using cutadapt; resulting reads shorter than 40bp were discarded. Reads for each sample, were aligned independently using TopHat2 (v2.0.10) (Kim et al., 2013) against the mouse genome (mm10). Counting proceeded over genes annotated in RefSeq release mm10, using htseq-count (version 0.6.1p1) (Anders et al., 2015). Only uniquely mapped reads were used to determine the number of reads falling into each gene (intersection-strict mode). Differential analysis was performed using DESeq2 package (1.6.3) (Anders and Huber, 2010). Differentially expressed genes, were determined by a p value of < 0.05 and absolute fold changes > 1.5 and max raw counts > 10.

Bioinformatics analysis

Differential expressed (DE) genes were analyzed with the use of Ingenuity Pathways Analysis (Ingenuity® Systems, https://www.ingenuity.com) to determine the most significantly relevant biological functions and pathways.

Telemetry probes implantation

Probe implantation was preformed according to the manufacturer's instructions (Huetteman and Bogie, 2009). Briefly, mice were anaesthetized with Ketamine (200 mg/kg BW) and xylazine (10 mg/kg BW). A midline incision was made on the ventral neck. The left common carotid artery was separated and ligated 1–2 mm cranially to its bifurcation. A second ligature was used to suspend the artery 4–5 mm proximal to the site of ligation. Through a small incision in the artery wall, the catheter was advanced 6–7 mm toward the aorta and fixed with sutures. A subcutaneous pocket on the flank of the animal was made with blunt scissors, and the transmitter was inserted therein using a small hemostat. The catheter and the transmitter were fixed in place with acrylic glue and the skin incision was closed with absorbable sutures. Mice were left to recover for 7 days after the surgery followed by 7 days of blood pressure recording. For stress induction, mice were introduced to a retired breeder ICR mouse for 20s and then separated with a barrier for another 24h.

Seizure Induction

Pentylenetetrazol (PTZ) was purchased from Sigma (Sigma P6500) and was dissolved in 0.9% NaCl to 3mg/mL. Seizures were induced with i.p. injection of 50mg/kg. Following injection, seizure behavior was followed for 30min. PTZ-induced seizures were classified by a six-point scale as was previously published (Westmark et al., 2008). Briefly, stage 0 was defined as no change in the behavior. Stage 1 was defined as hypoactivity, characterized by the animal being in a crouch or prone position with the abdomen fully touching the bottom of the cage. Stage 2 was defined as partial clonus, including that of the face, head, or forelimbs. Stage 3 was defined as generalized clonus, consisting of rearing, falling, and clonus of all four limbs and the tail, but with recovery. Stage 4 was defined as major seizures involving falls and staying down, exhibiting forelimbs that are parallel to the body axis and stiffness. Stage 5 was defined as major seizures involving hyperactivity, followed by a clonus of all four limbs that may end in death.

Behavioral studies-open field test

For behavioral tests mice were in a facility with reverse 12h light−dark cycle. All behavioral tests were performed during the dark phase of the cycle, following at least 1h of habituation. Before the restrain stress test, mice were placed in ventilated 50 mL Falcon tubes for 30 minutes. This test was performed as previously described (Volk et al., 2016). Briefly, the apparatus for the open-field test (TSE Systems) consists of a brightly illuminated (120 lux) white Plexiglas box (50 cm × 50 cm × 40 cm). Each mouse was placed in the corner of the apparatus to initiate a 10-min test session. A camera (Eneo model VK1316S) mounted above the apparatus, transmitted images of the mouse that were analyzed by VideoMot2 software (TSE Systems). Locomotion in the box was quantified using a video tracking system.

Brain tissue biopsies collection

Immediately after decapitation, mouse brains were removed and placed in 1.0 mm coronal slice intervals brain matrix (BSMAS001-1 Civic Instruments). The brains were sliced using standard razor blades into 2-mm slices that were frozen immediately on dry ice. The areas of interest were punched using a microdissecting 16G needle according to the anatomical references of The Mouse Brain in Stereotaxic Coordinates (Paxinos and Franklin, 2001). The brains were stored immediately at−80°C for later use.

Catecholamine measurements

Monoamines were extracted from the brain structures using 0.1 M perchloric acid. The extracts were assayed for Norepinephrine (NE), 3-Methoxy-4-hydroxyphenylglycol (MHPG), dopamine (DA), 3,4-dihydroxyphenylacetic acid (DOPAC), homovanillic acid (HVA) using reverse-phase high-performance liquid chromatography (RP-HPLC) with electrochemical detection (UltiMate3000/CoulochemIII; Thermo Fisher) using citrate-phosphate buffer (containing 6% acetonitrile 1% methanol, pH 4) as the mobile phase (Anderzhanova et al., 2013). Monoamines were separated on an analytical column (C18, 150 mm × 3 mm, 3 μm; Triart, YMC Europe) at a flow rate of 0.5 ml/min and detected at +220 mV and +350 mV. The detection limit for all compounds of interest was between 0.032 and 0.050 nM. Peak areas were used to calculate monoamine concentrations by reference to an external standard curve. Monoamine tissue contents were reported as micromoles per milligram of protein (the protein concentration of extracts was determined by the BCA method).

Immunostaining

In-vivo: Four-micrometer paraffin embedded tissue sections were deparaffinized by xylene and rehydrated through a gradient of ethanol. Sections were exposed to acetone for 7 min at −20°C and antigens were retrieved in citric acid in a microwave oven at full-intensity for 3 min until boiling point was reached, and then at 20% intensity for 10 min. Blocking of nonspecific binding was done with 20% normal horse serum and 0.2%–0.5% triton for 90 min in a humidity chamber. Sections were incubated with the primary antibodies as follow; ASL (1:100, Abcam, ab97370); TH (1:500, millipore AB1542). All antibodies were diluted in PBS containing 2% normal horse serum and 0.2% Triton. Sections were incubated overnight at RT followed by 48h at 4°C. Sections were washed three times in PBS and incubated with biotinylated anti-rabbit antibody for 90 min in a humidity chamber, washed, and incubated with streptavidin Cy2 and Cy3 anti-goat antibody (all from Jackson ImmunoResearch) for 40 min. Sections were counterstained by Hoechst (Molecular Probes). Stained sections were examined and photographed with a fluorescence microscope (Eclipse Ni-U; Nikon) equipped with Plan Fluor objectives (20x;40x) connected to a color camera (DS-Ri1, Nikon) microscope.

The fluorescence intensity quantification for the expression of TH was done blindly to the genotype using imageJ software.

Protein analysis: western blotting

Cells were lysed in RIPA and 1:100 protease inhibitor (Sigma-Aldrich). After centrifugation, the supernatant was collected, and protein content was evaluated by the BCA protein assay kit (Thermo Fisher 23225). 80μg of each sample under reducing conditions were loaded into each lane and separated by electrophoresis on a 10% SDS polyacrylamide gel. Following electrophoresis, proteins were transferred to Immobilon transfer membranes (Tamar). Non-specific binding was blocked by incubation with 5% milk in TBST (10 mM Tris–HCl (pH 8.0), 150 mM NaCl, 0.1% Tween 20) for 1 h at 25°C. Membranes were subsequently incubated with antibodies against ASL (1:500, ab97370, Abcam), p97 (1:10,000, PA5-22257, Thermo Scientific), GAPDH (1:1,0000, ab128915, Abcam), TH (1:500, CST-2792S, cell signaling). Antibody was detected using peroxidase-conjugated AffiniPure goat anti-rabbit IgG or goat anti-mouse IgG (Jackson ImmunoResearch) and enhanced using chemiluminescence western blotting detection reagents (Pierce ECL Western Blotting Substrate, Thermo Fisher). Gels were quantified by Gel Doc XR+ (BioRad) and analyzed by ImageLab 6.0 software (BioRad). The band area was calculated by the intensity of the band divided by the value obtained from the loading control.

RNA extraction and complementary DNA (cDNA) synthesis

RNA was extracted from cells using RNeasy Mini Kit (74104, QIAGEN). cDNA was synthesized from 1 μg RNA by using qScript cDNA Synthesis Kit (Quanta). Quantitative PCR was performed using SYBR green PCR master mix (Thermo Fisher scientific 4385612) or with TaqMan Real-Time PCR Master Mix (Thermo Fisher scientific 4444557). Primer sequences are summarized in the STAR Methods' Key Resources Table.

In situ hybridization

In situ hybridization procedures and probes were used as previously described (Korosi et al., 2006) with minor adjustments. Briefly, 500 base pair Antisense and sense (control) RNA probes were generated using *Asl* cDNA from mouse liver. The probe was designed to overlap the floxed region of the gene. The PCR products were cleaned by QIAquick PCR Purification Kit. The probe was incorporated into a plasmid containing T7/T3/SP6 RNA polymerase and transformed into DH5α competent cells. Following mini-prep, the DNA was sequenced to confirm insert identity and orientation. The plasmids were then linearized by PstI (antisense) and NcoI (sense) and following DNase treatment and purification, were added to the hybridization buffer.

Proteomic analysis

Samples from 100 cells collected from the LMD were digested by trypsin and analyzed by LC-MS/MS on Q Exactive plus (Thermo). The data was analyzed with MaxQuant 1.5.2.8 versus the Mouse Uniprot database. Data was analyzed using the same software. The identifications were filtered for proteins identified with FDR < 0.01 and that appeared in at least three samples in one group. As the proteins amount was low, identifications based on single peptides were not filtered out.

Flow cytometry for NO measurements

Dissections were performed on young mice (P20-P25) crossed with *Ai9*$^{f/f}$*; TH Cre*$^{+/-}$or *Ai9;Asl*$^{f/f}$*; TH Cre*$^{+/-}$mice. Single cell suspensions was made from mouse brain-stem region by enzymatic digestion with Papain Dissociation System (Worthington Biochemical) as was previously described (Feodorova et al., 2015). The cells were then analyzed by polychromatic flow cytometry. Data was acquired on an LSRII (BD Biosciences) and analyzed using BD FACSDiva 6 (version 7.6.5). Intracellular NO was detected by incubation of cells for 15 min at 37°C with 10 μM DAF-FM diacetate followed by extensive washing, according to the manufacturer's instructions (Molecular Probes).

Electrophysiology

Mice were rapidly decapitated, and the brains were removed and placed in 4°C low sodium sucrose-based cutting solution, containing (in mM): 2.5 KCl, 16 NaHCO3, 1.25 NaH2PO4, 10 glucose, 10 MgSO4, 0.5 CaCl2 and 234 sucrose. 350 um coronal slices containing the LC region were prepared in the same solution using a vibro-slicer. Slices were then transferred into ACSF containing

(in mM): 124 NaCl, 2.5 NaH2PO4, 26 NaHCO3, 2.7 MgSO4, 2.7 KCl, 19 glucose, 2 ascorbic acid and incubated at 37°C for 45 minutes. Following incubation, slices were kept and recorded at room temperature. Slices and solutions were constantly carbogenated (5% CO2 and 95% O2). Slices were then transferred to a recording chamber placed on the stage of an Olympus BX51WI upright microscope and perfused with ACSF at approximately 1.5mL/min. Single LC neurons were visualized using infrared Nomarski optics and recorded with patch pipettes containing (in mM): 136 K-gluconate, 10 KCl, 5 NaCl, 10 HEPES, 0.1 EGTA, 0.3 Na-GTP, 1 Mg-ATP, and 5 phosphocreatine, pH 7.2, having a resistance of 5–10 MOhm. Signals were amplified with Axopatch 200A and recorded with PClamp-10 (Axon Instruments). Data was analyzed offline using Clampfit 10, MATLAB R2017b and Microsoft Excel 2016.

Spikes (threshold, peak and after hyperpolarization) were detected using a homemade script based on numerical derivative. Spike characteristics were obtained from average of over 10 spikes per recording, aligned at peak. After hyperpolarization, recovery slope was calculated as a maximal change over 3ms period in 80ms window after the peak. Inter spike intervals (ISI) were calculated as distances between consecutive spike peaks. Histograms were constructed with a step calculated from the 1st and 3rd quartiles of ISI distributions and aligned at mean ISI, averaged histogram is presented in Figure 5.

QUANTIFICATION AND STATISTICAL ANALYSIS

Unless indicated otherwise, values are expressed as mean ± SEM. Statistical analysis was performed by Weizmann statistician using repeated-measures two-way ANOVA with Bonferroni post hoc t tests or Student's t tests as appropriate. Statistical details of individual experiments such as exact values of n can be found in the figures and legends. The sample size was chosen in advance based on common practice of the described experiment, and is mentioned for each experiment. Each experiment was conducted with biological and technical replicates and repeated at least three times unless specified otherwise. Statistical tests were done using Prism software (GraphPad Software). $p < 0.05$ was considered significant in all analyses (* denotes $p < 0.05$, **$p < 0.005$, ***$p < 0.0005$, **** $p < 0.0001$).

DATA AND CODE AVAILABILITY

The RNA sequencing data are published with Gene Expression Omnibus (GEO). The accession number is GEO: GSE138471